

# Landslide Susceptibility Mapping with GIS-Based Conditional Adversarial Networks

Mohamed Mafaz  
BTech Artificial Intelligence and Data science  
Crescent Institute of Science and Technology  
Chennai, India  
mohdmafaz200303@gmail.com

Akul Pradeep  
BTech Artificial Intelligence and Data science  
Crescent Institute of Science and Technology  
Chennai, India  
akulpral2@gmail.com

Dr. Aisha Banu W  
Head of Department CSE  
Crescent Institute of Science and Technology  
Chennai India  
hodcse@crescent.education

**Abstract**—A landslide is the movement of a mass of rock, debris, or earth down a slope. Landslides are a type of “mass wasting,” which denotes down-slope movement of soil and rock under gravity [1]. In India, about 0.42 million sq. km or 12.6% of land area, excluding snow covered area, is prone to landslide hazard [2]. Landslide susceptibility mapping is the process of identifying areas prone to landslides amid natural changes to that of the geology, tropical factors, environmental factors and many more. In process of mapping these regions and classifying them into different categories of threat level, it help in early detection and avoidance. By using EOBrowser [3] to quickly view and analyze different algorithms, this paper shows promise of easier and accurate landslide mapping. After Mapping of existing landslide cases, those cases where taken in during Data Collection process further fed into Conditional Adversarial Network for prediction of LSM before it happens. During data collection process various factors where cross referenced and: NDVI, dNDVI, Slope, Elevation, NDWI, Barren soil index where ranked as the most important one of them all.

**Keywords**—*Landslide susceptibility mapping, EOBrowser, NDVI, dNDVI, Slope, Elevation, NDWI, Barren soil index.*

## I. INTRODUCTION

There exist multiple factors that can cause landslide or are in many cases a prominent contributing factor that directly relates to landslide. Paper “Selection of contributing factors for predicting landslide susceptibility using machine learning and deep learning models” [4] brings forward many of these factors such as: Lithology, Plan, Profile, STI, Aspect, Distance to fault, NDVI, Distance to stream, Rainfall, Distance to road, SPI, TWI, Slope, Elevation, Land use.

Thought our implementation and experimentations we found out that NDVI, dNDVI, Slope, Elevation, NDWI, Barren soil index are enough to give high accuracy. NDVI, dNDVI, NDWI, Barren soil index are retrieved from Sentinel satellite via API and Slope and elevation maps are retrieved from Copernicus DEM (Digital Elevation Model). Scripts writing in EOBrowser gives instant preview of LSM but the final rendering of LSM happens on codebase where other factors such as dNDVI (which is difference Normalized Vegetation Index) that cannot be calculated as dNDVI requires multi-temporal (multi-date) analysis, while EO Browser primarily processes data for single timestamps at a time are applied.

Further more Conditional Adversarial model was build around it inheriting the basic skeleton of “Image-to-Image Translation with Conditional Adversarial Networks” paper. This paper was designed to accept on image as guidance, tailoring this model to fit our requirement required us to modify the input mechanism that allowed multiple images to be accepted as inputs, that leads to the generating of a mask,

better understanding of images and faster convergence since the original models where found.

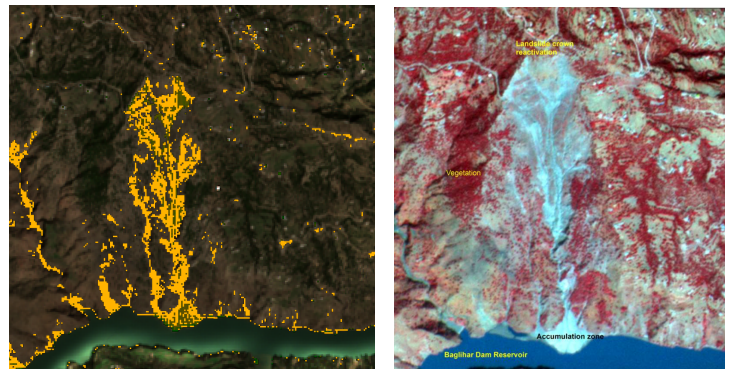


Fig. 1. Our algorithm vs Landslide Atlas of India [1]

## II. UNDERSTANDING FACTORS

### A. NDVI

NDVI is a remote sensing index used to measure and monitor vegetation health and density. It compares the difference between the near-infrared (NIR) and red light reflected by vegetation [6]. NDVI values range from -1 to +1, where:

- Higher values (closer to +1) indicate healthy, dense vegetation.
- Lower values (closer to 0 or negative) indicate bare soil, water, or non-vegetated areas.

$$\text{NDVI} = \frac{\text{NIR} - \text{Red}}{\text{NIR} + \text{Red}}$$

(1)

### B. NWDI

The Normalized Difference Water Index (NDWI) is used to monitor changes in water content of vegetation, bodies of water, and soil. It is similar to NDVI but instead of focusing on vegetation, it targets the presence of water. NDWI uses green and near-infrared (NIR) bands to detect water bodies and moisture levels in vegetation [7].

$$\text{NDWI} = \frac{\text{Green} - \text{NIR}}{\text{Green} + \text{NIR}}$$

(2)

### C. dNDVI

dNDVI (Differential NDVI) refers to the change in NDVI values between two different time points (dates),

which allows for the detection of temporal variations in vegetation health, growth, and other environmental factors.

Unlike NDVI, which is a snapshot of vegetation at a single time, dNDVI measures the difference in vegetation over time, providing valuable insights into vegetation dynamics. This is especially useful in agricultural monitoring, climate change studies, and land cover analysis.

$$d\text{NDVI} = \text{NDVI}_{t_2} - \text{NDVI}_{t_1} \quad (3)$$

Where  $\text{NDVI}_{t_2}$ , NDVI value at the second time point (later date) and  $\text{NDVI}_{t_1}$ , NDVI value at the first time point (earlier date). Positive dNDVI values indicate an increase in vegetation or greening. Negative dNDVI values indicate decreasing vegetation or browning.

dNDVI is crucial for masking where False Positive regions in terms of pixel values can be eliminated when dNDVI is used as a mask, as loss of vegetation is one of the primary indication of landslide occurred regions or fire occurred regions [8] when it comes to remote monitoring.

#### D. Slope

Slope refers to the steepness or degree of incline of a surface, typically expressed as the ratio of vertical change (rise) to horizontal distance (run). In geographic and environmental contexts, slope is an essential factor in understanding landforms, hydrology, and potential natural hazards.

$$\text{Slope} = \frac{\text{Vertical Change (Rise)}}{\text{Horizontal Distance (Run)}} \quad (4)$$

#### E. Slope

Slope refers to the steepness or degree of incline of a surface, typically expressed as the ratio of vertical change (rise) to horizontal distance (run). In geographic and environmental contexts, slope is an essential factor in understanding landforms, hydrology, and potential natural hazards.

#### F. BSI (Bare Soil Index)

The Bare Soil Index (BSI) is a vegetation index specifically designed to help identify bare soil areas in remote sensing imagery. It is particularly useful in monitoring land surface changes, soil moisture, and detecting areas of vegetation cover or lack thereof.

Different bands capture various wavelengths of light reflected by the Earth's surface. Vegetation, for example, reflects most of the near-infrared light (B08), while bare soil and non-vegetated surfaces tend to reflect more of the shortwave infrared light (B11) and red (B04) wavelengths.

$$BSI = \frac{(B11 + B04) - (B08 + B02)}{(B11 + B04) + (B08 + B02)} \quad (5)$$

- Positive BSI values (when B11 and B04 dominate over B08 and B02) indicate bare soil or non-vegetated areas. Higher BSI values suggest that the area has a higher presence of exposed soil.
- Negative or low BSI values (when B08 and B02 dominate over B11 and B04) indicate vegetated areas, where the vegetation is actively reflecting near-infrared light.

- Zero values or close to zero typically suggest mixed land surfaces or areas where vegetation and soil are equally present.

### III. SCRIPTS FORMATION AND INFERENCES

Sentinel bands and data			
Band	Name	Wavelength (nm)	Resolution
B01	Coastal Aerosol	442.7 (S2A), 442.3 (S2B)	60m
B02	Blue	492.4 (S2A), 492.1 (S2B)	10m
B03	Green	559.8 (S2A), 559.0 (S2B)	10m
B04	Red	664.6 (S2A), 665.0 (S2B)	10m
B05	Vegetation Red Edge	704.1 (S2A), 703.8 (S2B)	20m
B06	Vegetation Red Edge	740.5 (S2A), 739.1 (S2B)	20m
B07	Vegetation Red Edge	782.8 (S2A), 779.7 (S2B)	20m
B08	NIR (Near-Infrared)	832.8 (S2A), 833.0 (S2B)	10m
B8A	Narrow NIR	864.7 (S2A), 864.0 (S2B)	20m
B09	Water vapour	945.1 (S2A), 943.2 (S2B)	10m
B11	SWIR (Shortwave Infrared)	1613.7 (S2A), 1610.4 (S2B)	20m
B12	SWIR (Shortwave Infrared)	2202.4 (S2A), 2185.7 (S2B)	60m

Table 1: Sentinel Band's data, [9]

#### A. Cloud Detection

Cloud poses threats when data needed is of specific dates, i.e before and after the occurrences of landslides. The closer the range of data gathered, the better. Two major reasons of why data might be inaccessible at required intervals: Clouds presences blocks the ability of satellite to pickup meaning full data and hinders with set up algorithms, Satellite simply doesn't orbit over that particular region on the date.

The detection and avoidance of clouds are handled using a combination of the B11 (SWIR band) and B03 (Green band) values, alongside the bRatio calculation. Here's a breakdown of the formula and logic used to identify clouds:

- a) *Initial Cloud Detection Criteria:* This calculates the ratio of the Green band (B03) values after normalizing between a range of 0.175 to 0.39. This ratio helps in distinguishing between vegetation, water, and clouds

$$b\text{Ratio} = \frac{B03 - 0.175}{0.39 - 0.175} \quad (5)$$

- b) *Cloud Check Condition:* The check for clouds is based on B11 (SWIR band) and the bRatio.

$$\text{Cloud Detected} = \begin{cases} \text{True} & \text{if } (B11 > 0.1) \wedge (b\text{Ratio} > 0.001) \\ \text{True} & \text{if } (B11 > 0.1) \wedge (b\text{Ratio} > 0) \wedge (\text{NDGR} > 0) \\ \text{False} & \text{otherwise} \end{cases}$$

NDGR stands for Normalized Difference Green Ratio. It is a ratio-based index that typically measures the difference between the green band and another band (often the red band), with normalization to standardize the values.

$$\text{NDGR} = \frac{\text{B03} - \text{B04}}{\text{B03} + \text{B04}}$$

(6)

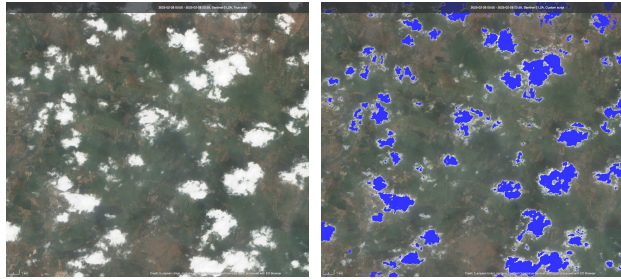


Fig. 2. Clouds vs Cloud detection using Custom Script.

### B. Water body Detection

Water Body is detected using the NDWI factor itself without much tweaking.



Fig. 3. Water body vs Water body detection using Custom Script.

### C. dNDVI

As mentioned in equation (3), the dNDVI is calculated by subtracting later date NDVI with earlier date NDVI, or the vice versa depending on the need.

This is crucial in landslide or forest fire detection task as it is a vital point from analysis point of view. By finding dNDVI we can create a mask as mentioned before.

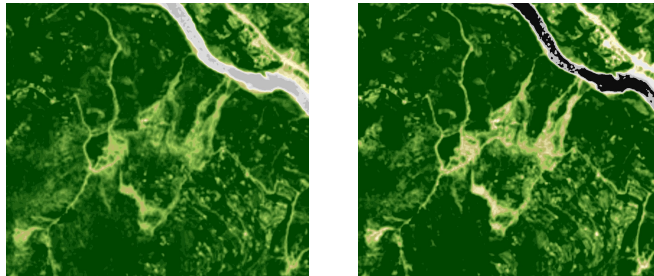


Fig. 4. NDVI before landslide (2024-05-01) vs NDVI after landslide (2024-05-16). Pernote Village.



Fig. 5. dNDVI Mask, NDVI (after landslide) - NDVI (before landslide)

By subtracting and making sure only to keep those pixels who's NDVI (after landslide) is lighter (lower value) than that of NDVI (before landslide), to make sure the mask obtained is of vegetation decreasing and not vegetation increasing [10].

### D. Landslide probable areas

The identification of landslide-prone areas was based on a combination of high BSI, low NDVI, and specific thresholds of the B11 band. The criteria for marking an area as potentially prone to landslides are as follows:

High shortwave infrared values ( $\text{B11} > 0.8$ ): Suggests dry, non-vegetated land, which is typically more vulnerable to sliding, especially during heavy rainfall.

Low NDVI values ( $\text{NDVI} < 0.15$ ): Indicates a lack of vegetation, which further exacerbates the potential for landslides, as vegetation helps to anchor the soil and prevent erosion.

High BSI values ( $\text{BSI} > 0.1$ ): Exposed soil areas with high BSI values are more prone to instability, as they lack the protective cover of vegetation.

If all these conditions are met, the area was flagged as a potential landslide zone. The special color coding [1.5, 0.7, -1] was applied to these pixels to visualize them in a manner that highlighted their susceptibility to landslides.

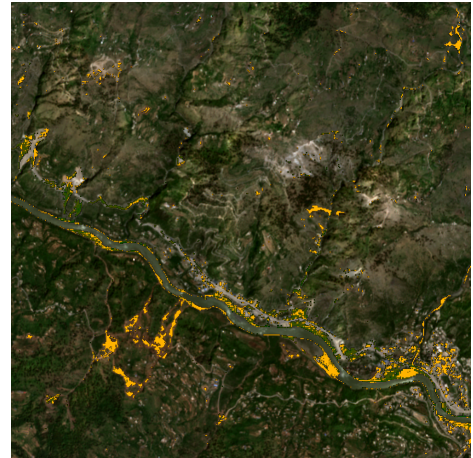


Fig. 6. Landslide in Pernote Village without dNDVI Masking. [11]

After applying the mask from Fig 4, the regions with False Positives were diminished and much refined areas were targeted :

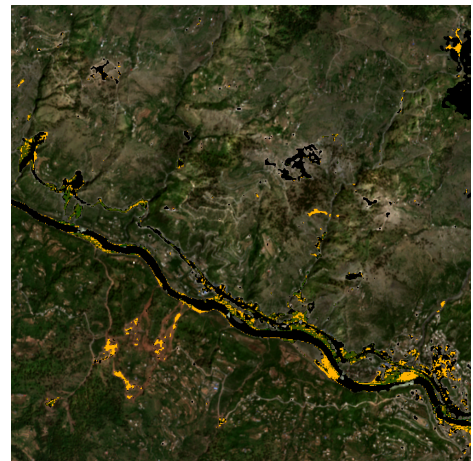


Fig. 7. Landslide in Pernote Village with dNDVI Masking.

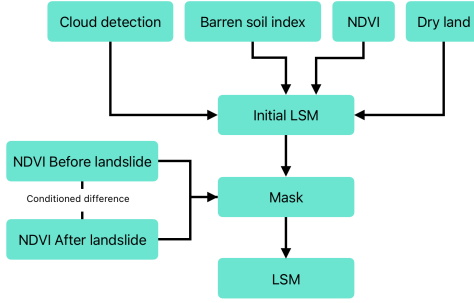


Fig. 8. Landslide Susceptibility mapping algorithm.

#### IV. CONDITIONAL ADVERSARIAL NETWORK

CGANs are an enhanced version of GANs where both the generator and discriminator are conditioned on some additional information. This helps guide the generation process making it more controlled and targeted.

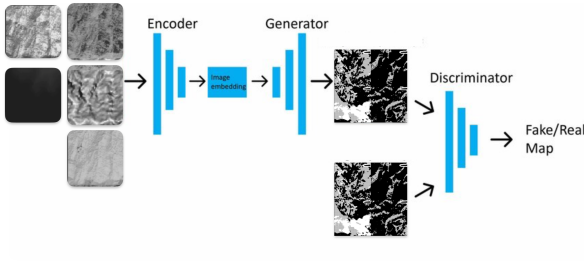


Fig. 9. Training a conditional GAN that takes in, Gray image, NDVI, NDWI, Elevation, Slope as inputs, the generator learns to fool the discriminator.

The objective of the cGAN comes out to be

$$\mathcal{L}_{cGAN}(G, D) = \mathbb{E}_y[\log D(C, y)] + \mathbb{E}_z[\log(1 - D(C, G(C, z)))] \quad (7)$$

$C$  is a vector of conditions of arbitrary length  $n$ , i.e.,  $C = (c_1, c_2, \dots, c_n)$ .

In our case  $n$  is 5, i.e. the number of input to the cGAN is 5, additional images can be added but there is a need of staying alert as there will be a saturation point that a certain number of input the Conditions can become counterproductive.

We use L1 loss just like the paper, that is Lasso (Least Absolute Shrinkage and Selection Operator), this encourages sparsity, meaning it tends to drive some coefficients exactly to zero.

Our final objective is:

$$G^* = \arg \min_G \max_D \mathcal{L}_{cGAN}(G, D) + \lambda \mathcal{L}_{L1}(G) \quad (8)$$

We use PatchGAN – that only penalizes structure at the scale of patches. This discriminator tries to classify if each  $N \times N$  patch in an image is real or fake. We run this discriminator convolutionally across the image, averaging all responses to provide the ultimate output of  $D$ .

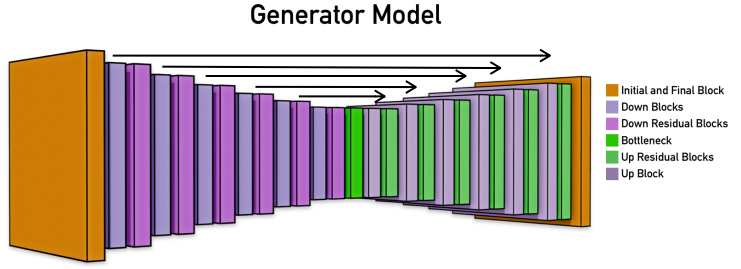


Fig. 10. Generator model, mostly remains same as that of “Image-to-Image Translation with Conditional Adversarial Networks” paper, the initial and final blocks are modified to fit our use case.

#### Discriminator Model

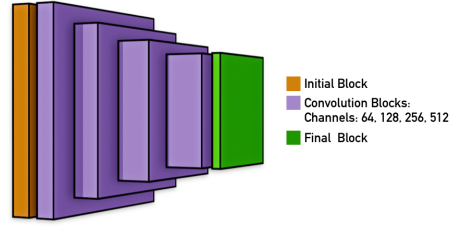


Fig. 11. Discriminator model, remains same as that of “Image-to-Image Translation with Conditional Adversarial Networks” paper.

A defining characteristic of image-to-image translation problems is that they map a high-resolution input grid to a high-resolution output grid. Moreover, for the problems we consider, the input and output differ in their surface appearance, yet they both represent the same underlying structure. Consequently, the structure in the input is roughly aligned with the structure in the output. Considering these factors, we design the generator architecture accordingly.

Many previous solutions to problems in this domain have employed an encoder-decoder network. In such a network, the input is processed through a series of progressively downsampling layers until a bottleneck layer is reached. At this point, the process is reversed. However, this network requires that all information flow through all layers, including the bottleneck. For numerous image translation problems, there is a significant amount of low-level information shared between the input and output. It would be advantageous to directly transmit this information across the network. For instance, in the case of image colorization, the input and output share the location of prominent edges.

#### V. DATASET CREATION

Dataset creation was another tedious part of the process and redialing available dataset didn't fit our requirements. To accomplish this we got NASA's Dataset for landslides [14], out of which the columns we felt relatable were: event\_date (The date on which the landslide occurred), event\_title (brief title describing the event), latitude, longitude.

##### A. Data Filtering Criteria

To ensure relevance and temporal consistency, the dataset is filtered to include only landslide events that occurred between January 1, 2018, and 10 days before the date of data collection. This filtering process eliminates outdated data and ensures that the analysis is based on recent events and the reason being for 2018 to be the start of our

scraping is that sentinel satellites became operational after 2017, and consistent somewhere around late 2017.

### B. Automating Grid Scan Algorithm

The way we approach to fetch giant piece of land for scanning when required and scaling is back down for various requirements and to loose as little data as possible we use grid and access each grid in sequential order. Further advancements can be made by parallelizing this approach.



Fig. 11. An example of how our grid scan algorithm segments a piece of land (southern india for reference).

The reason for the first row of the grid to be above the user defined longitude and longitude is that during our analysis we constantly using grid of 1x1 for scanning smaller pieces of land, which made sense when longitude and latitude were bottom left, this approach can be altered but this is what we stuck to.

The algorithm used in the function to add distance to each grid is a latitude-longitude grid generation algorithm based on Vincenty's formulae or Haversine-based calculations approximations for small distances. Specifically, it: Assumes the Earth as a sphere (radius = 6,371,000 meters) and uses simple trigonometric approximations to compute shifts in latitude and longitude:

$$\Delta\text{lat} = \frac{\text{distance}}{R} \times \frac{180}{\pi} \quad (9)$$

Longitude change ( $\Delta\text{lon}$ ) is computed using:

$$\Delta\text{lon} = \frac{\text{distance}}{R \times \cos(\text{latitude})} \times \frac{180}{\pi} \quad (10)$$

This accounts for the fact that longitude degrees get compressed as you move towards the poles.

A discovery was made that could cause potential hurdles in creating dataset, and that was clouds. Clouds pose a threat to proper retrieval of images and since our dataset was supposed to consist of images predominantly, this issue needed to be addressed.

To solve this issue following steps were carried out:

a) *Get dates before and after the landslide that the sentinel satellite flew over:* There is a small window when the satellite flies over the desired region, being every 5-6 days, using Copernicus's Catalog API [15] it made it possible to fetch us 5-6 dates before and after the landslide occurred over the region.

b) *Get Cloud coverage for each date:* Using the same Copernicus's Catalog API, for the list of 10-12 dates fetched, each dates are looked up via the api and assigned a percentage of cloud coverage.

c) *Find the optimal date:* Two dates that is closest to the landslide occurring date, one for before landslide occurring and other for after landslide occurred.

User has the option of whether to apply these steps for each grid separately or altogether, for this paper we chose to apply these steps for each grid.

Since different grids might select different dates, this can lead to visual discontinuities in the final composite image. If uniformity is critical (e.g., for seamless mosaicking), setting false ensures all grids use the same date, even if cloud coverage varies. If minimizing cloud cover is the priority, enabling the feature will optimize individual grids at the cost of continuity.

By balancing temporal consistency and cloud-free visibility, users can configure the algorithm based on their specific needs.

### C. Mapping gathered as projects

CSV file from NASA were downloaded from which the columns were filtered as discussed above and the dates were also filtered as discussed above.

Images gathered from sentinel satellite using custom scripts include projects of which each project consists of :

- a) *NDVI\_Before:* NDVI before the landslide.
- b) *NDVI\_After:* NDVI after the landslide.
- c) *True\_Color\_After:* True Color After the landslide.
- d) *LSM\_Only\_After:* Only the LSM markings after the landslide
- e) *Mask:* Conditional subtraction between NDVI after the landslide and NDVI Before the landslide.
- f) *LSM\_True\_Colour\_Masked:* LSM merged with True Color and masked with the previous masking.
- g) *Log\_file:* Consisting information such as dimension resolution, latitude, longitude, dates etc.

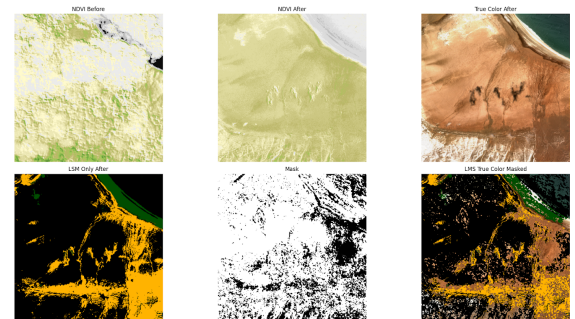


Fig. 12. Data within anyone of the project files.

From these projects, (around 900 were scrapped), the dataset were made:

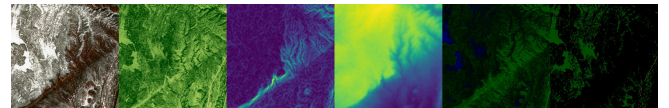


Fig. 13. U.S. 14\_16\_20 Rockslide at Tunnel.



Fig. 14. Yeshwantpur-Karwar Express Landslip.

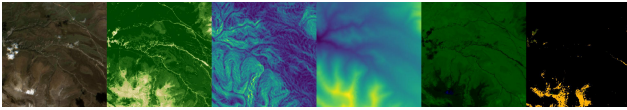


Fig. 15. Westside Rd Landslide Evacuates Killiney Beach Residents.

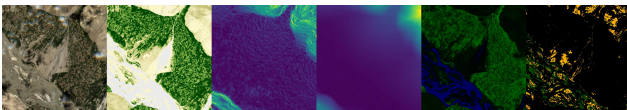


Fig. 16. Wat Khae Tham Phra Landslide.

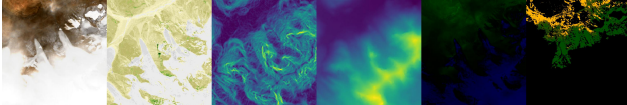


Fig. 17. Yedekumeri Railway Station.

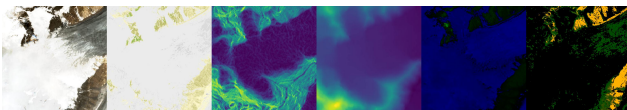


Fig. 18. Vidyagiri Residency Landslide.

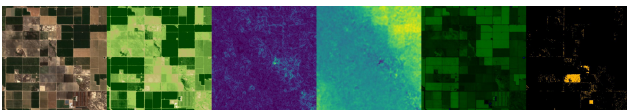


Fig. 19. Wagamon Road Landslide in Teekkoy.

All these were gathered using sentinel hub api [17], and the dataset (above images) are in order of:

a) *Base Image*: The original satellite image capturing the study area in natural color or bands.

b) *NDVI (Normalized Difference Vegetation Index)*: Measures vegetation health by analyzing the difference between near-infrared (NIR) and red light reflectance.

c) *Slope*: Represents the steepness or incline of terrain, derived from elevation data, critical for assessing landslide susceptibility.

d) *Elevation*: The height of the terrain above sea level, influencing water runoff and stability of slopes.

e) *NDWI (Normalized Difference Water Index)*: Identifies water bodies by measuring the difference between shortwave infrared (SWIR) and near-infrared (NIR) reflectance.

f) *LSM (Landslide Susceptibility Map) Only*: A processed output highlighting regions prone to landslides based on terrain and environmental factors; it is also the ground truth (something to be predicted).

## VI. MODEL TRAINING

Model training isn't much different from the Pix2Pix paper but few more metrics have been incorporated into it such as Style loss; Style loss is commonly used in style transfer and GAN-based image generation tasks to ensure that the generated images preserve the texture, patterns, and high-level structure of a reference style image. It is based on the VGG network and was originally introduced in the Gatys et al. (2016) style transfer paper [18].

The style loss is computed as the mean squared error (MSE) between the Gram matrices of the generated image  $\hat{I}$  and the target style image  $I_s$ :

$$\mathcal{L}_{style} = \sum l_w_i ||G_{\hat{I}}^l - G_{I_s}^l||^2$$

where:

- $F_{ik}$  represents the activation of the  $i^{th}$  feature map at position k.

- The Gram matrix captures the correlations between different feature maps, representing the overall style of an image.

## VII.

## EVALUATION

When comparing images, the mean squared error (MSE)—while simple to implement—is not highly indicative of perceived similarity. Structural similarity aims to address this shortcoming by taking texture into account. [18] [19] [20]. The SSIM is designed to improve on traditional metrics like PSNR and MSE, which have proved to be inconsistent with human eye perception. Based on human visual system.

The SSIM (Structural Similarity Index Measure) formula evaluates the perceptual similarity between two images or volumes by considering luminance, contrast, and structure. The formula is:

$$SSIM(x, y) = [l(x, y)]^\alpha * [c(x, y)]^\beta * [s(x, y)]^\gamma \quad (11)$$

Where:

$l(x, y)$  is the luminance comparison,

$c(x, y)$  is the contrast comparison,

$s(x, y)$  is the structural comparison, and

$\alpha$ ,  $\beta$ , and  $\gamma$  are positive constants, typically set to 1 in practice.

The luminance comparison  $l(x, y)$  is calculated as:

$$l(x, y) = (2 * \mu_x * \mu_y + C1) / (\mu_x^2 + \mu_y^2 + C1) \quad (12)$$

The contrast comparison  $c(x, y)$  is calculated as:

$$c(x, y) = (2 * \sigma_x * \sigma_y + C2) / (\sigma_x^2 + \sigma_y^2 + C2) \quad (13)$$

And the structural comparison  $s(x, y)$  is calculated as:

$$s(x, y) = (\sigma_{xy} + C3) / (\sigma_x * \sigma_y + C3) \quad (14)$$

Where:

$\mu_x$  and  $\mu_y$  are the means of the two images/volumes,

$\sigma_x$  and  $\sigma_y$  are the standard deviations,

$\sigma_{xy}$  is the covariance, and

$C1$ ,  $C2$ , and  $C3$  are constants, usually set to  $(K1 * L)^2$ ,  $(K2 * L)^2$ , and  $C2 / 2$  respectively, where  $K1$  and  $K2$  are small constants (e.g., 0.01 and 0.03) and  $L$  is the dynamic range of the image.

Accuracy of the model trained is 0.899.

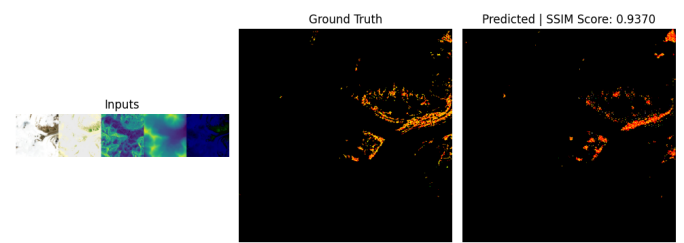


Fig. 20. Kattipara Landslide.

## REFERENCES

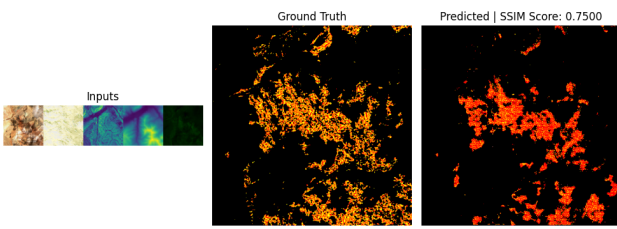


Fig. 21. Kot Village Landslide in Tehri District.

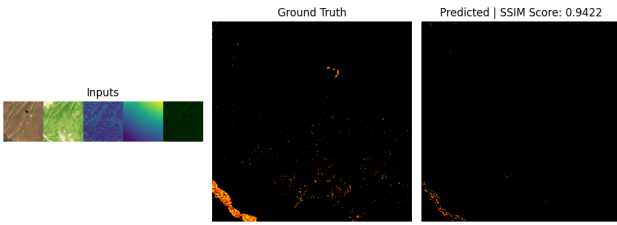


Fig. 22. Hpakant Jade Mining Region Landslide.

## VIII. CONCLUSION

This study presents a novel approach to landslide susceptibility mapping by leveraging a Conditional Generative Adversarial Network (cGAN) architecture, adapted from Pix2Pix, and enhanced to accept multi-channel input derived from satellite imagery. By integrating key geospatial indicators—such as dNDVI, BSI, NDWI, elevation, and slope—the model effectively learns spatial patterns associated with landslide-prone regions. The inclusion of temporal vegetation dynamics (dNDVI) and land surface characteristics (BSI, NDWI) provides an enriched context that improves the model’s predictive capacity.

Experimental results demonstrate that the proposed model outperforms traditional binary classification methods by capturing complex nonlinear relationships and spatial dependencies inherent in landslide occurrences. The generated susceptibility maps align closely with known landslide locations, underscoring the potential of GAN-based architectures in geospatial hazard prediction tasks.

Future work will explore the integration of additional dynamic environmental variables (e.g., rainfall, soil moisture) and the use of higher-resolution datasets to further enhance predictive accuracy. The results of this research highlight the promise of deep generative models in environmental monitoring and disaster risk management, offering scalable tools for data-scarce and high-risk regions.

1. Nirmala Jain, Priyom Roy, Tapas Ranjan Martha, Punit Jalan and Aishwarya Nanda (2023). Landslide Atlas of India (Mapping, Monitoring and R&D studies using Remote Sensing data). NRSC special publication. NRSC/ISRO. Document
2. Geological Survey of India, "Landslide Hazard Zonation Map," Bhukosh, [Online]. Available: [https://bhusanket.gsi.gov.in/LS\\_hazard.html](https://bhusanket.gsi.gov.in/LS_hazard.html). [Accessed: Apr. 15, 2025].
3. U.S. Geological Survey, "What is a landslide and what causes one?" USGS, Oct. 26, 2022. [Online]. Available: <https://www.usgs.gov/faqs/what-a-landslide-and-what-causes-one>. [Accessed: Mar. 2, 2025].
4. Geological Survey of India, "Landslide Hazard," GSI, 2025. [Online]. Available: [https://www.gsi.gov.in/webcenter/portal/OCBIS/pages\\_pageGeoInfo/pageLANDSLIDEHAZRD](https://www.gsi.gov.in/webcenter/portal/OCBIS/pages_pageGeoInfo/pageLANDSLIDEHAZRD). [Accessed: Mar. 2, 2025].
5. Sentinel Hub, "EO Browser," Sentinel Hub, 2025. [Online]. Available: <https://www.sentinel-hub.com/explore/eobrowser>. [Accessed: Mar. 2, 2025].
6. Cheng, Chen & Fan, Lei. (2023). Selection of contributing factors for predicting landslide susceptibility using machine learning and deep learning models. Stochastic Environmental Research and Risk Assessment. 10.1007/s00477-023-02556-4
7. Phillip Isola, Jun-Yan Zhu, Tinghui Zhou, Alexei A. Efros, "Image-to-Image Translation with Conditional Adversarial Networks," 2018, arXiv:1611.07004 . [Online]. Available: <https://doi.org/10.48550/arXiv.1611.07004>
8. NASA Earth Observatory, "Measuring Vegetation: The Normalized Difference Vegetation Index (NDVI)," \*NASA\*, 2025. [Online]. Available: <https://earthobservatory.nasa.gov/features/MeasuringVegetation>. [Accessed: Mar. 2, 2025].
9. EOS Data Analytics, "NDWI – Normalized Difference Water Index," \*EOS\*, 2025. [Online]. Available: <https://eos.com/make-an-analysis/ndwi/>. [Accessed: Mar. 2, 2025].
10. Fire Severity and Vegetation Recovery on Mine Site Rehabilitation Using WorldView-3 Imagery - Scientific Figure on ResearchGate. Available from: [https://www.researchgate.net/figure/Difference-Normalised-Difference-Vegetation-Index-dNDVI-analysis-of-WorldView-3-images\\_fig4\\_326165995](https://www.researchgate.net/figure/Difference-Normalised-Difference-Vegetation-Index-dNDVI-analysis-of-WorldView-3-images_fig4_326165995) [accessed 2 Mar 2025]
11. Sentinel Hub, "Sentinel-2 L2A Data," Sentinel Hub Documentation. [Online]. Available: <https://docs.sentinel-hub.com/api/latest/data/sentinel-2-l2a/> [Accessed: Mar. 2, 2025].
12. Ganerød, A. J., Franch, G., Lindsay, E., & Calovi, M. (2024). Automating global landslide detection with heterogeneous ensemble deep-learning classification. Science of the Total Environment, 874, 158383. <https://doi.org/10.1016/j.scitotenv.2023.158383>
13. Landslide Blog, "Peru's Pernote Landslide," The Landslide Blog, Dec. 18, 2020. [Online]. Available: <https://eos.org/thelandslideblog/pernote-landslide-1>. [Accessed: Mar. 2, 2025].
14. Juang CS, Stanley TA, and Kirschbaum DB (2019) Using citizen science to expand the global map of landslides: Introducing the Cooperative Open Online Landslide Repository (COOLR). PLOS ONE 14(7): e0218657. doi:10.1371/journal.pone.0218657
15. Copernicus Data Space Ecosystem, "Catalogue APIs," [Online]. Available: <https://dataspace.copernicus.eu/analyse/apis/catalogue-apis>. [Accessed: Apr. 15, 2025].
16. Sentinel Hub, "Sentinel Hub API," Sinergise Ltd., Accessed: Apr. 15, 2025. [Online]. Available: <https://www.sentinel-hub.com/develop/api/>
17. Leon A. Gatys, Alexander S. Ecker, and Matthias Bethge, "A Neural Algorithm of Artistic Style," arXiv preprint arXiv:1508.06576, 2015. [Online]. Available: <https://doi.org/10.48550/arXiv.1508.06576>
18. Scikit-Image, "Structural Similarity Index (SSIM) — skimage v0.25.0 documentation," Accessed: Apr. 15, 2025. [Online]. Available: [https://scikit-image.org/docs/0.25.x/auto\\_examples/transform/plot\\_ssim.html](https://scikit-image.org/docs/0.25.x/auto_examples/transform/plot_ssim.html)
19. Zhou Wang; Bovik, A.C.; , "Mean squared error: Love it or leave it? A new look at Signal Fidelity Measures," Signal Processing Magazine, IEEE, vol. 26, no. 1, pp. 98-117, Jan. 2009.
20. Z. Wang, A. C. Bovik, H. R. Sheikh and E. P. Simoncelli, "Image quality assessment: From error visibility to structural similarity," IEEE Transactions on Image Processing, vol. 13, no. 4, pp. 600-612, Apr. 2004.